GMOS-S optical spectroscopy of LMC SNRs to reveal the [P II] knot origins

Rommy Aliste C.[1], Ji Yeon Seok[2], Yong-Hyun Lee[3], Dongkok Kim[1], Bon-Chul Koo[1]
[1]Seoul National University, [2]Korea Astronomy and Space Science Institute, [3]Samsung SDS
contact: Rommy Aliste Castillo, rommy@astro.snu.ac.kr

1. Introduction

• Observational studies of SN feedback are limited. The location of galactic SNRs and the distance to extragalactic SNRs makes them difficult to explore.

• The LMC is a unique place to study SN feedback due to its proximity and location. This allows the structure of SNRs and their environment to be investigated in some detail.

• Recently, we conducted a study of 13 LMC SNRs using [P II] (1.189 μm) and [Fe II] (1.257 μm) narrowband imaging obtained with SIRIUS/IRSF. We derived P/Fe abundance ratios (X(P/Fe)) using the [P II]/[Fe II] line ratio, and three SNRs (N206, N157B and N158A) show X(P/Fe) comparable or even higher than those of general ISM.

• The galactic SNR Cas A exhibits high X(P/Fe) due to the enhanced P abundance (Koo et al. 2013). However, we lack a clear explanation for the LMC SNRs (i.e., SN ejecta, CSM/ISM or contamination from nearby sources).

2. SNR Targets

• **N206** is an old (25 kyr) and large (44 pc) mixed-morphology SNR located northeast of an H II region. While its optical emission reveals a circular, limb-brightened structure, its IR emission may be affected by its surroundings. The [P II] and [Fe II] line maps show a weak and extended emission, and a small bright clump in the south of the remnant.

• **N157B** lies within an H II region and is one of the largest Crab-like SNRs (29 pc). [P II] and [Fe II] emissions are diffuse and extended, but spatially mismatched with X-ray emission. Its complex environment affects the discrimination of SNR materials.

• **N158A** is one of the well-known Crab-like SNRs and contains a PWN. It has been classified as oxygen-rich, presumably from ejecta. The [P II] and [Fe II] emissions are concentrated in a clump in the center of the remant, where the pulsar and a bright time-variable structure ("blob") are located.

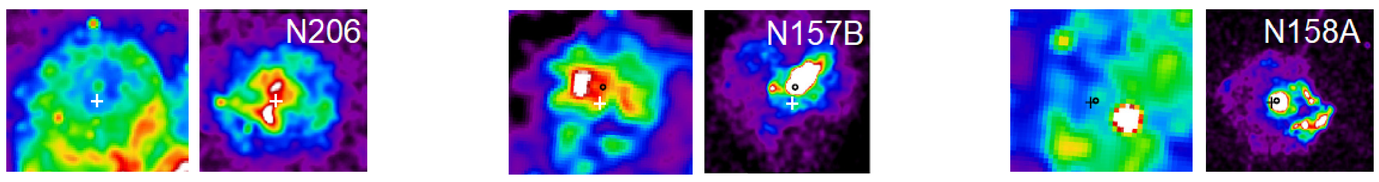

Figure 1. SNR targets are shown on MCELS Hα (*left*) and Chandra X-ray (*right*) images.

4. Observations: Optical spectra

• We conducted the spectroscopic observations using GMOS-S mounted on the Gemini-South telescope in November 2020 (GS-2020B-Q-234). We used a long-slit configuration covering 3800-7000 Å, with a slit size of 1" (width) × 330" (length). We performed the data reduction using PyRAF for longslit spectra.

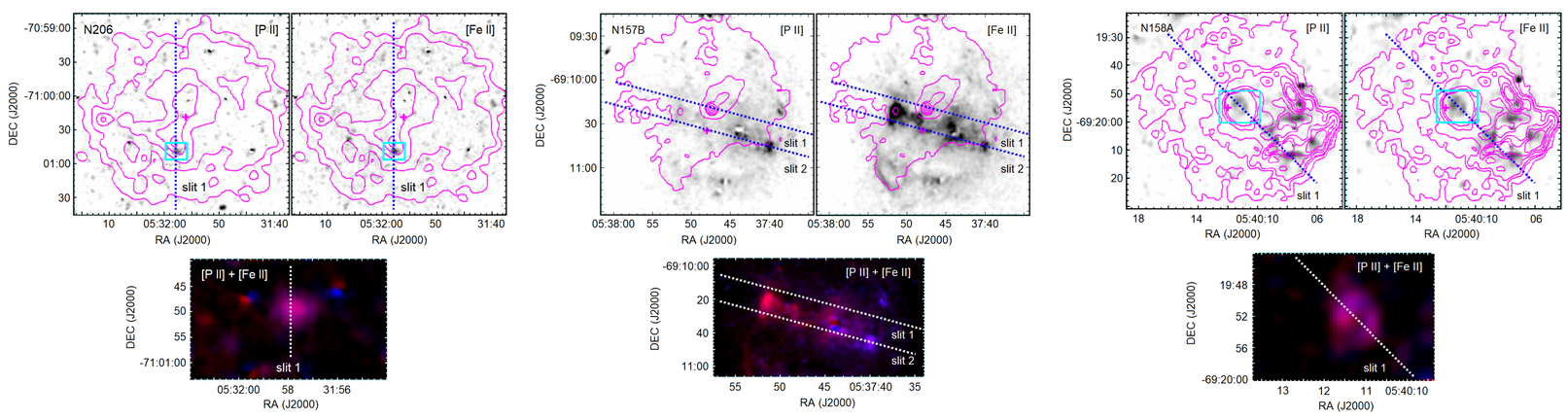

Figure 2. In the panels, SNR images of [P II] - 1.19 μm and [Fe II] - 1.26 μm obtained using SIRIUS/IRSF are shown (Aliste et al. in prep.). X-ray contours from Chandra are overlapping. The cross marks indicate the center of the SNRs. Below are the color composite images of [P II] (blue) and [Fe II] (red), along with the slit positions. Gaussian kernels of 3 sigma were used to smooth all the images.

5. Results

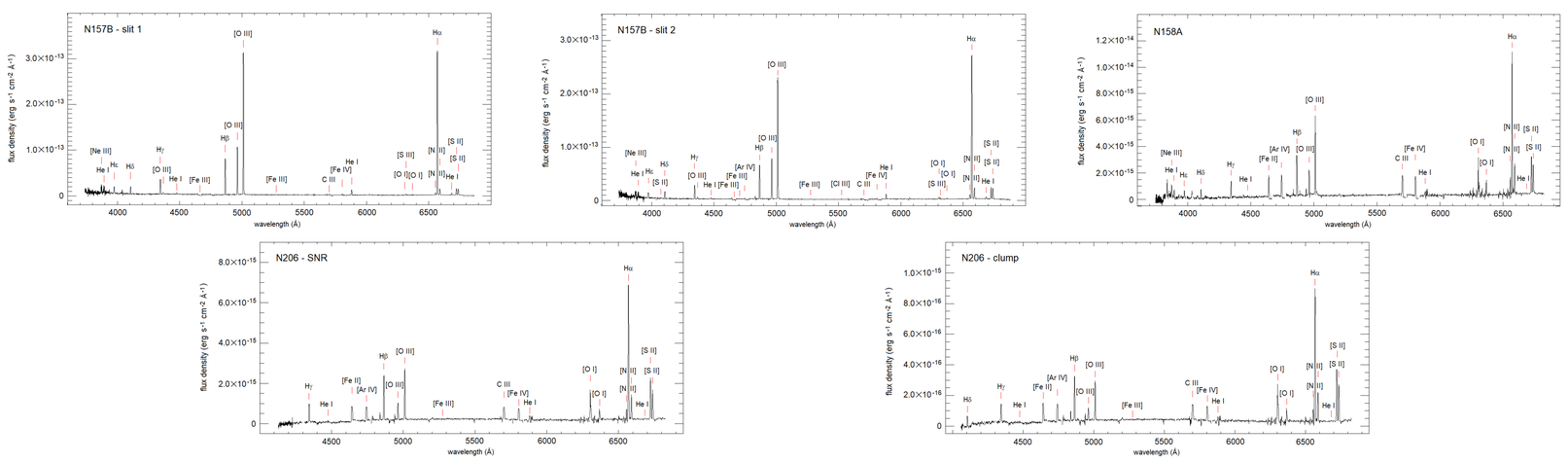

Figure 3. Panel show the GMOS-S spectra of the three SNRs. For N206, two spectra are extracted, one for the whole SNR and the other for the central clump. N206 - clump emission lines are similar to those in N206 - whole SNR, except for the ratio between Hβ and [O III] 5007Å. Furthermore, N157B - slit 2 exhibits emission lines that are not present in N157B - slit 1 (e.g., [S II] 4069Å, [Fe III] 4702Å, [Ar IV] and [Cl III]).

Table 1. Various diagnostic line ratios measured from the GMOS-S spectra. These indicate that the ratios of N157B tend to differ from those of the other two SNRs. The electron densities can be derived from [S II] I(6716Å)/I(6731Å) line ratios. The smaller [S II] line ratios may indicate denser regions.

Line Ratios	N206 SNR	N206 clump	N158A	N157B slit 1	N157B slit 2
He I/Hα	0.04	0.05	0.04	0.04	0.04
[S II]/Hα	0.57	0.72	0.54	0.09	0.18
[O I]/Hα	0.21	0.26	0.13	0.01	0.02
[N II]/Hα	0.26	0.31	0.34	0.07	0.12
[O III]/Hβ	1.13	0.87	1.82	3.93	3.61
[S II]$_{(6716/6731)}$	1.36	1.36	1.27	1.04	1.04

3. Objective

• Reveal whether the origin of [P II] knots is due to SN ejecta, CSM/ISM or contamination from nearby sources based on the analysis of [N II], He I and H I emission lines, and estimate the shock velocities using shock models.

6. Shock Modeling

- We use the shock code MAPPINGS V shock code to build self-consistent pre-ionization radiative shock models for shock velocities from 100 to 475 km s^{-1} (Sutherland & Dopita, 2017).

- We adopt an abundance set of 0.5× the Local Galactic Concordance values. We also choose other abundance sets at various logarithmic Fe depletion factors in the range -0.25 to -1.00.

- For each velocity, the pre-shock density varies to keep the ram pressure of the shock constant (P_{ram} = 1.5×10^{-7} dynes cm^{-2}).

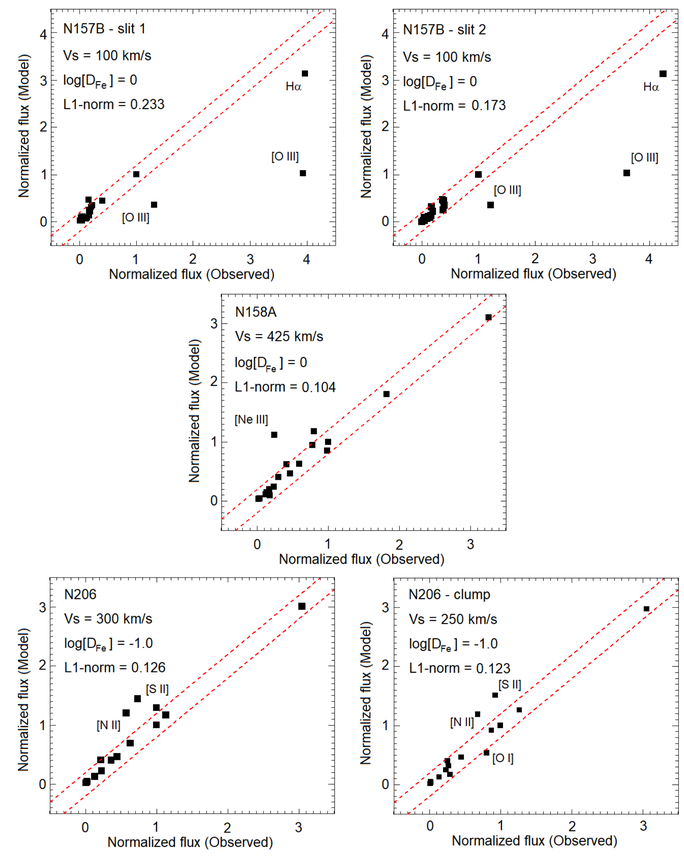

Figure 4. Comparison on the modeled and observed line fluxes for more than a dozen emission lines, where Flux (Hβ) = 1.0. The red dashed lines represent a difference between the model and the observation of ±20%. The L1-norm minimization corresponds to the modulus of the mean logarithmic difference in flux between the model and the observations. The observed line ratios can be reasonably fitted by a shock model, although some lines deviate substantially from it.

7. Summary

According to the line ratios, SNR N157B differs from the other two SNRs. N157B's line ratios are reasonably fitted by a shock of 100 km s^{-1}. As a preliminary conclusion, SNR N157B emissions can be contaminated by nearby sources due to the complexity of the environment, making it difficult to separate them from SNR emissions. In addition, as a result of the velocity estimates, the possibility of SN ejecta causing high emissions of [P II] can be ruled out. The N abundance can be used in future work to determine if knots are CSM or ISM.

References

1. Aliste et al., in prep.; 2. Dickey & Lockman, 1990, ARA&A, 28, 215; 3. Dickel et al. 1994, AJ, 107, 1067; 4. Dopita et al. 2018, ApJS, 237, 10; 5. Fesen et al. 2008, ApJS, 174, 379; 6. Kaaret et al. 2001, ApJ, 546, 1159; 7. Koo et al. 2013, Science, 342, 1346; 8. Micelotta, Brandl & Israel, 2009, A&A, 500, 807; 9. Sutherland & Dopita, 2017, ApJS, 229, 34; 10. Williams et al. 2005, ApJ, 628, 704.